Blockers of VacA Provide Insights into the Structure of the Pore

Francesco Tombola,* Giuseppe Del Giudice,† Emanuele Papini,‡ and Mario Zoratti*

*Censiglio Nazionale delle Ricerche, Centro Biomembrane and Dipartimento di Scienze Biomediche, Università di Padova, Padova; †Centro Ricerche Istituto Ricerche Immunologiche Siena, CHIRON S.p.A., Siena; and ‡Dipartimento di Scienze Biomediche e Oncologia Umana, Università di Bari, Bari, Italy

ABSTRACT The cytotoxic effects of the *Helicobacter pylori* toxin VacA, an important etiogenic factor in human gastric diseases, are due to its ability to form anion-selective pores in target cell membranes. We have studied the inhibition of channel activity by 5-nitro-2-(3-phenylpropylamino) benzoic acid (NPPB) and 4,4′-diisothiocyanatostilbene-2,2′-disulfonic acid (DIDS), representatives of two popular classes of chloride channel blockers, to gain information on the mechanism of blocking and on the unknown structure of the VacA pore. The data indicate that both compounds produce a fast block by binding to separate but mutually exclusive sites within the channel lumen. DIDS binds close to the pore opening on the side of protein insertion, whereas NPPB blocks at a position in the opposite half of the channel. Although DIDS reaches the blocking site by traveling along the lumen, inhibition by NPPB appears to involve mainly partition of the compound into the membrane, voltage-independent diffusion from it to the inhibitory position, and voltage-dependent exit. The data are consistent with a pore that can be more easily entered from the side of protein insertion than from the opposite end.

INTRODUCTION

VacA, a toxin produced by *Helicobacter pylori* (Cover and Blaser, 1992; Montecucco et al., 1999), is responsible for the vacuolating effect exerted on a variety of mammalian cell lines by the supernatant obtained from cultures of this bacterium (Leunk et al., 1988). It causes alterations in protein traffic (Satin et al., 1997), reduces the transepithelial resistence (TER) of model epithelia (Papini et al., 1998; Pelicic et al., 1999) and is believed to be an important factor in the genesis of the widespread gastroduodenal diseases associated with *H. pylori* (Telford et al., 1994). The mature, secreted toxin forms hexamers or heptamers with a ring structure and a central depression (Lupetti et al., 1996; Cover et al., 1997; Lanzavecchia et al., 1998; Czajkowsky et al., 1999). Isolated VacA becomes active upon preexposure to acidic (de Bernard et al., 1995) or alkaline (Yahiro et al., 1999) pH. This treatment induces the dissociation of oligomers into monomers, which expose hydrophobic portions allowing their insertion into lipid bilayers, where they reassemble into supramolecular structures (de Bernard et al., 1995; Cover et al., 1997; Molinari et al., 1998, Czajkowsky et al., 1999). Secreted VacA has been shown (Garner and Cover, 1996) to bind to the host cell surface and to be slowly internalized and delivered to acidic compartments (late endosomes and lysosomes), which give rise to vacuoles in the presence of permeant amines (Papini et al., 1994, 1997; Molinari et al., 1997).

The isolated, acid-activated toxin has recently been shown to form anion-selective, low-conductance, voltage-dependent channels (Tombola et al., 1999a; Szabò et al., 1999; Iwamoto et al., 1999). We have provided evidence that pore formation by VacA is closely associated with toxin-induced vacuolation and TER decrease (Szabò et al., 1999; Tombola et al., 1999a,b). This conclusion was based, among other evidence, on the observed strict correlation between the inhibition by a set of chloride channel inhibitors of VacA-mediated current conduction through planar bilayers and HeLa cell plasma membrane and the toxin's effects on cells and epithelia. Our current working model of VacA-induced vacuolation envisions the formation of anion-selective channels in the membrane of late endosomal compartments by the internalized toxin. The increased permeability to anions would result in increased proton pumping by the electrogenic V-ATPase, accumulation of osmotically active ammonium salts (in the presence of permeable amines) in the endosomal lumen, swelling, and subsequent homotypic fusion to produce vacuoles (Tombola et al., 1999a; Szabò et al., 1999).

In the literature, most of the compounds we investigated as VacA inhibitors have been consistently described as blockers. The most powerful (on VacA) of them, 5-nitro-2-(3-phenylpropylamino) benzoic acid (NPPB), presents some interesting features, which depend on the specific channel being studied and which differentiate it from other blockers such as DIDS. To mention just a few examples, currents most probably carried by the volume-activated ClC-3 channel were inhibited by NPPB in a voltage-independent manner, whereas the effect of DIDS on the same channel was voltage-dependent (Schmid et al., 1998; von Weikersthal et al., 1999; Dick et al., 1998). The same behavior was displayed by Ca^{2+}-activated artery endothelial chloride currents (Nilius et al., 1997). Similarly, the currents recorded after injecting *Xenopus* oocytes with a rabbit ClC-2 cRNA construct were inhibited by NPPB with little or no influence of voltage (Furukawa et al., 1998). In

Received for publication 20 January 2000 and in final form 17 May 2000.

Address reprint requests to Mario Zoratti, CNR C. S. Biomembrane, Dipartimento Scienze Biomediche, Viale Giuseppe Colombo 3, 35121 Padova, Italy. Tel: +39-049-8276054; Fax: +39-049-8276049; E-mail: zoratti@civ.bio.unipd.it.

0006-3495/00/08/863/11 $2.00

this case extracellular DIDS had no effect. On the other hand, e.g., the anion currents elicited in *Xenopus* oocytes by injection of xClC-5 (Schmieder et al., 1998), hpICln and hClC-6 (Buyse et al., 1997) cRNA, believed due to an endogenous conductance activated by the expression of any one of these proteins, were inhibited by both NPPB and DIDS in a voltage-dependent manner (Schmieder et al., 1998). The extent of inhibition was side-of-addition-dependent in some cases (Tilmann et al., 1991), but not in others (Singh et al., 1991). At the single-channel level, NPPB produced, for example, a decrease of the observed channel conductance, interpreted as a fast block, in the case of an outwardly rectifying chloride channel from colonic enterocytes (Singh et al., 1991). A slower, flicker-type block was observed, for example, in the case of an outwardly rectifying chloride channel from a human colon carcinoma cell line and respiratory epithelial cells (Tilmann et al., 1991) and of a volume-activated endothelial Cl^- channel (Nilius et al., 1994). Studies accounting for these differences and clarifying the underlying mechanistic variants are lacking. VacA thus represented a good model system for an investigation of this type. In the case of this channel, the titration curve relating current conduction to [NPPB], as well as those obtained with two other fenamates and with R(+)-2-[(2-Cyclopentenyl-6, 7-dichloro-2, 3-dihydro-2-methyl-1-oxo-1H-inden-5-yl)oxy]acetic acid (IAA-94), has two components, the minor one of which represents a residual, hard-to-inhibit conduction (Tombola et al., 1999b).

We have studied the inhibition of VacA pores by NPPB and by 4,4′-diisothiocyanatostilbene-2,2′-disulfonic acid (DIDS), to obtain indirect structural information on the channel using the blockers as probes, and to clarify the mechanisms involved, which may also apply in other cases.

MATERIALS AND METHODS

VacA was purified from *H. pylori* strain CCUG 17874, as described (Manetti et al., 1995; Tombola et al., 1999a), and used after preactivation by exposure to low pH in planar bilayer experiments conducted as previously reported (Tombola et al., 1999a,b). Perfusion of the chambers to eliminate added toxin was not normally performed, because it entailed a high risk of membrane loss. In this paper the *cis* compartment is defined as the one containing the active electrode, whose voltage relative to ground (in *trans*) is reported. The *cis* compartment was also, unless otherwise specified, the chamber into which the toxin was added, the toxin addition side (TAS). Current (cations) flowing from the *cis* to the *trans* side was considered positive and plotted upward. The planar membrane was formed by diphytanoyl-phosphatidylcholine (DPhPC; Avanti Polar Lipids, Alabaster, AL). The experimental media contained 0.5 M KCl unless otherwise specified, plus 0.5 mM $CaCl_2$ and $MgCl_2$, and 10 mM Hepes/K^+, pH 7.2. Single-channel experiments were conducted with a 4:1 [KCl] gradient (*cis*: 2.0 M; *trans*: 0.5 M), and the toxin and inhibitors were added to the *trans* compartment. The side of toxin addition in these experiments was chosen, in view of the voltage dependence of the channels (Tombola et al., 1999a), to maximize the current flowing at positive (*cis*) voltages. Despite this, in the presence of inhibitor the apparent single channel conductance at $V > 0$ could be reliably determined in only a few experiments. Sources and stock solutions of the inhibitors used were as described by Tombola et al. (1999b).

Determination of the pKa of NPPB

The equilibrium constant for the dissociation of NPPBH was obtained (as shown in Fig. 1, curve *a*) by plotting the concentration of NPPB versus pH according to the relationship:

$$[NPPB^-]/C = 1/(1 + 10^{(pKa-pH)}) \quad (1)$$

where C is the total concentration of NPPB in solution, i.e., $C = [NPPB^-] + [NPPBH]_{sol}$. $[NPPB^-]$ was determined spectrophotometrically from the absorbance of solutions at the peak wavelength, $\lambda = 412$ nm ($\epsilon = 15{,}000$ $l \cdot mol^{-1} \cdot cm^{-1}$), assuming a unitary activity coefficient. NPPB from a stock dimethylsulfoxide solution was added to aliquots of 0.5 M KCl, 10 mM citrate/K^+, 10 mM phosphate/K^+, 10 mM HEPES having pH values (adjusted with KOH) between 3.0 and 8.0, to a nominal concentration $C_o = 50$ μM. After overnight equilibration, any NPPBH precipitated (in the lower pH range) was removed by centrifugation, and the absorbance of aliquots of the supernatants was measured. The pH of these solutions was then brought to 8.0 by adding predetermined volumes of Tris solution to cause the complete dissociation of the acid, and the absorbance was measured again to determine C.

RESULTS

Current conduction by a channel may well be decreased by uncharged permeating molecules (e.g., Bezrukov et al., 1994; Linsdell and Hanrahan, 1996), but the term "open channel block" is often used to refer to the binding of a charged species to a site or sites within the pore, resulting in

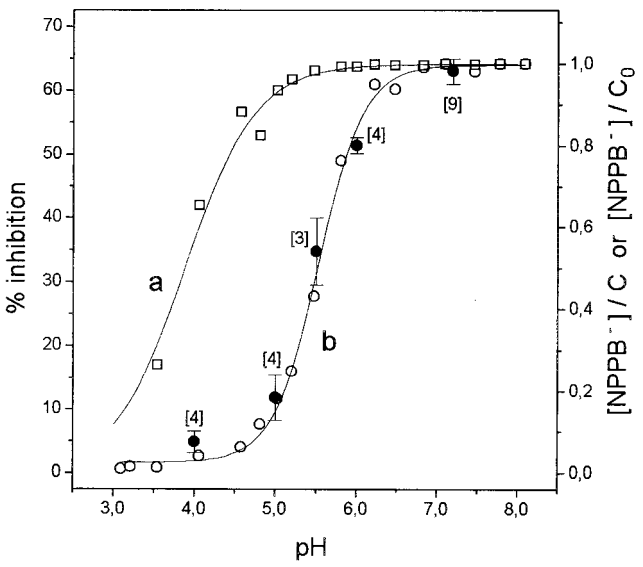

FIGURE 1 Acid/base equilibrium of NPPB and inhibition of current conduction as a function of pH. The concentration of NPPB anion, $[NPPB^-]$, in nominally 50 μM solutions was determined as a function of pH as indicated in Materials and Methods. The measured values, divided by either the total concentration of NPPB in solution ($C \equiv [NPPB^-] + [NPPBH]_{sol}$; □, curve *a*) or by 50 μM (C_0; ○, curve *b*) are plotted versus pH. The percentage of inhibition of current conduction by VacA (V: −40 mV; 500 mM KCl medium) by nominally 50 μM NPPB (*cis*) at various medium pH values is also shown (●; numbers in brackets refer to the number of experimental values averaged; error bars, ±SE). See text for details.

a decreased current flow while the binding lasts. Since we propose that inhibition of vacuolation by this and other compounds descends from a block of VacA channels in the late endosomal membrane, it was of interest to determine whether a large fraction of NPPB can exist as the anion at the pH values thought to prevail in late endosomes (pH $\approx$ 5–6; e.g., Alberts et al., 1994; Altan et al., 1999). We therefore determined the previously unknown pKa of NPPB as described in Materials and Methods, obtaining a value of 3.9 $\pm$ 0.1 from the best fit of curve *a* in Fig. 1. Thus, $NPPB^-$ is expected to be the predominant form in solution at pH $>$ 4. We next sought to establish a correlation between the extent of channel inhibition and [$NPPB^-$] or [NPPBH] in solution. As shown by curve *b* in Fig. 1, plots of [$NPPB^-$] versus pH and of percent of channel inhibition versus pH were superimposable within experimental error. However, because of the low solubility of the undissociated acid in aqueous media, in these experiments, which employed a concentration of NPPB (50 μM) causing considerable inhibition at pH 7, a precipitate started to form as the pH was lowered below about 6. Given the presence of the solid, in the acidic range a constant and low ($\approx$0.5 μM) concentration of NPPBH was present. The accuracy of our data does not allow us to distinguish whether channel inhibition correlates with [$NPPB^-$] or with ([$NPPB^-$] + $[NPPBH]_{sol}$). It is clear, though, that it does not correlate with $[NPPBH]_{sol}$.

We next performed single-channel experiments, illustrated in Fig. 2. VacA channels display slow and fast gating modes: closed times in the several millisecond range separate longer periods of fast bursting activity (Fig. 2, *A–D*). The slow gating is voltage-independent (Tombola et al., 1999a). Within bursts, most transitions cannot be fully resolved even at filter corner frequencies of 5 KHz. Single channel currents ($i_{s.ch.}$) could, however, be measured from relatively long-lasting events using high filter cutoff frequencies (3–5 KHz) and sampling rates (20–50 KHz). For simplicity, we assume here that VacA can adopt only one current-conducting state. Records such as those exemplified in Fig. 2, *C* and *D*, suggest that within bursts, the open probability of the uninhibited channel was not far from 0.5 (see also Iwamoto et al., 1999). The presence of NPPB results in an apparent decrease of the channel conductance (compare traces A and B with traces C and D, Fig. 2). Full-size current steps could still be identified using high filter settings in the presence of 10 μM NPPB, but not with 50 μM inhibitor (not shown). Fig. 2, *E* and *F*, presents current amplitude histograms derived from longer stretches of the records illustrated by Fig. 2, *A* and *B*, fitted with the sum of two gaussian distributions. The larger peak represents the current conducted by the bursting channel. The smaller one, close to i = 0, collects the baseline, closed-channel current, and its presence is due mainly to the relatively long closed periods due to the slow gating mode. The shift toward zero in the position of the bursting current

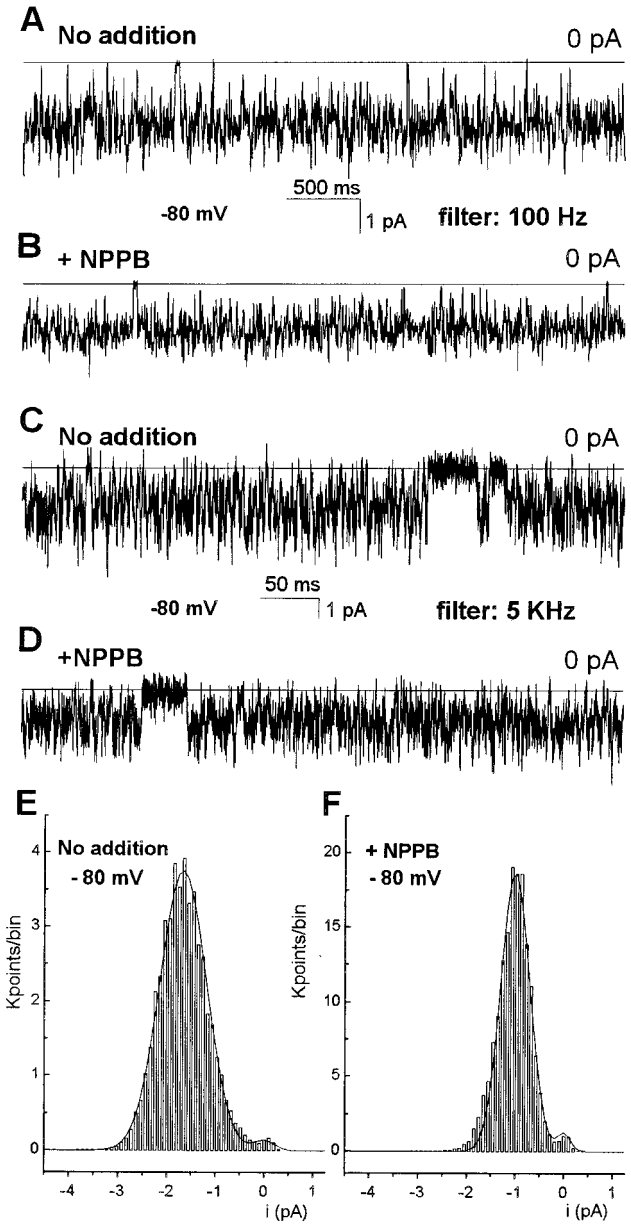

FIGURE 2 Inhibition of single-channel current conduction by NPPB. Experiments with 2.0 M KCl in the *cis* compartment and 0.5 M KCl in *trans*. Pre-activated VacA was added to the *trans* compartment. Illustrative current traces recorded in the absence (*A*) or presence (*B*) of 50 μM NPPB in the *trans* compartment. The same channel was active in (*A*) and (*B*). Filter: 100 Hz. Digital sampling: 1 KHz. V: $-$80 mV. (*C*) and (*D*) Traces from the same experiment as in (*A*) and (*B*), filtered at a corner frequency of 5 KHz and sampled at 50 KHz. (*E*) and (*F*) Amplitude histograms obtained from longer sections of the record illustrated in (*A*) and (*B*), respectively.

amplitude peak, i.e., of the mean current conducted by the channel, can be plausibly accounted for by a reduction of the channel open probability (P_o), according to the relationship $\langle i_{s.ch.} \rangle = i_{s.ch.} P_o$. P_o here indicates the probability of finding the channel in the current-conducting state, i.e.,

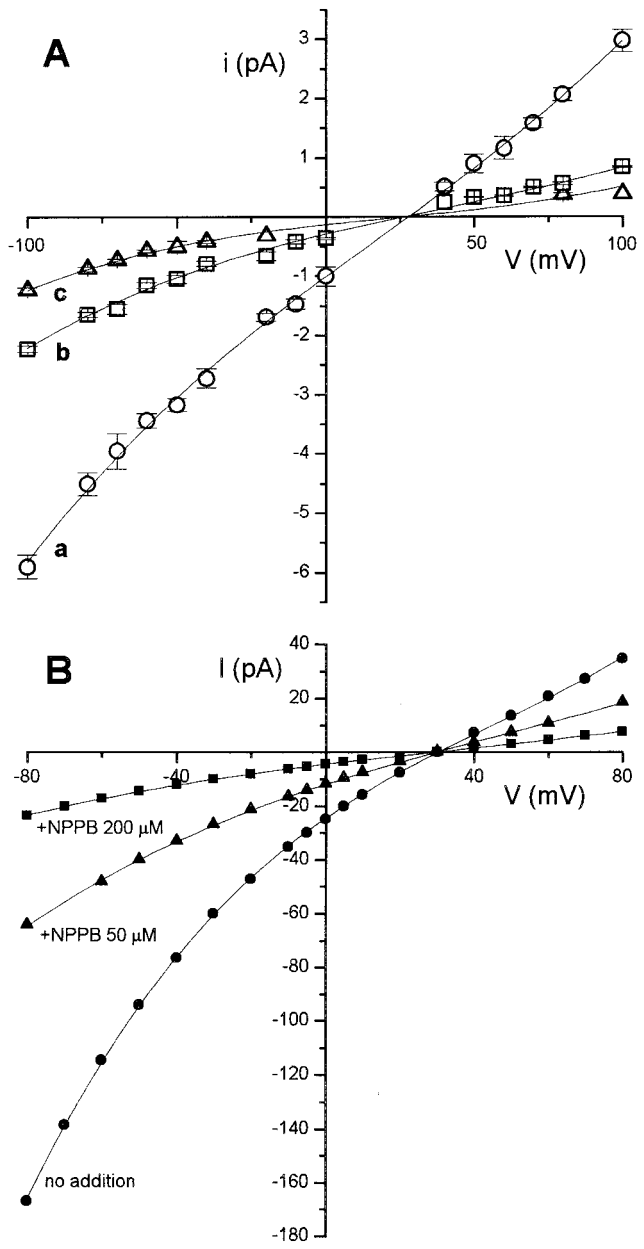

FIGURE 3 Selectivity with and without NPPB. (*A*) Single-channel I/V plots. In all cases the medium was 2:0.5 M (*cis:trans*) KCl. The toxin and NPPB were added to the *trans* compartment. Curve *a*: No inhibitor added. Amplitude data were obtained from direct measurements of some of the longest-lasting events in current traces recorded with a filter cutoff frequency of 4 KHz and a sampling frequency of 20 KHz. At least 10 independent determinations from 4 separate esperiments were averaged for each point. Error bars represent standard deviations. Curves *b* and *c*: The data are the difference between the peaks of gaussian distributions corresponding to the baseline current (closed/blocked channel) and to the current conducted by the bursting channel (see Fig. 2, *E* and *F*). Curve *c* was obtained in the presence of 50 μM NPPB (*trans*). The points plotted are the mean values, $\pm$SE, obtained by averaging 4 to 21 determinations of the current at a given voltage in the presence (*c; triangles*) or absence (*b; squares*) of inhibitor, except for the values at +40 mV in curve *b*, and at −20 and +100 mV in curve *c*, which are single determinations. The interpolations are third-order polynomial fits of all the individual data (not of the averages). The original current records were filtered at 200 Hz and sampled at 1 KHz. (*B*) I/V plot from a representative multi-channel experiment conducted in 390:100 mM (*cis:trans*) KCl. Toxin and inhibitor at the concentrations indicated were added to the *cis* compartment.

$P_o = 1 - P_{closed} - P_{blocked}$. The shift in the presence of the inhibitor is accompanied by a reduction of the histogram's width, i.e., of the standard deviation of the mean current, σ. This effect can be rationalized on the basis of the relationship (e.g., Verveen and De Felice, 1974):

$$\sigma^2 = i^2_{s.ch.} P_o (1 - P_o) \quad (2)$$

The plot of this function is a parabola with its maximum at $P_o = 0.5$. If the P_o of the uninhibited channel is $\approx$0.5, its reduction due to blocking is expected to result in a decrease of σ. At present it cannot be completely excluded (but see below) that NPPB binding causes only a decrease, rather than a complete block, of current conduction by the channel. In this case the reduction of σ might be accounted for by this decrease. Within this hypothesis, the residual, hard-to-inhibit current flowing at high concentrations of NPPB (Fig. 2 in Tombola et al., 1999b) would be carried by the channels in this partially inhibited state, whose conductance would be approximately 12% of the uninhibited level.

The effects of NPPB are consistent with a fast open channel block. Alternatively, 1) the blocker might bind in the channel lumen determining only a partial reduction of the ion flux without grossly altering the gating kinetics, or 2) NPPB might bind to an external site determining either the partial or the complete closure of the pore with fast characteristics. Although these alternatives cannot be completely excluded, they are made unlikely by the results and considerations presented below.

We determined whether the selectivity of the channels partially inhibited by NPPB differed significantly from that exhibited by the untreated channels. This would not be expected to be the case if the current in the presence of NPPB is carried only by a fraction of unblocked, i.e., inhibitor-free, channels. If, instead, NPPB acted according to hypothesis 1) above, the presence of an anion in the channel lumen might affect this property. Fig. 3 *A* shows single-channel I/V plots obtained by plotting averaged amplitudes determined from current traces recorded at high filter cutoff frequencies (curve *a*, *circles*), or from the peak of gaussian fits analogous to those shown in Fig. 2, *E* and *F*, without (curve *b*, *squares*) and with (curve *c*, *triangles*) 50 μM NPPB. The channel remains anion-selective in the presence of the inhibitor, though the lack of data in the most relevant region did not allow a precise determination of the reversal potential in single-channel experiments. In multi-channel experiments (Fig. 3 *B*), the reversal potentials in the presence of NPPB were close to the value obtained with uninhibited channels under the same conditions (31 $\pm$ 2

mV; Tombola et al., 1999a). We observed E_{rev} shifts of -0.8 ± 0.6, -2.4 ± 1.0, and -3.2 ± 1.5 mV with 50, 200, and 500 μM NPPB, respectively ($n = 3$). Variations of this magnitude are within the combined experimental error and can be plausibly accounted for by the formation of a more negative surface potential because of NPPB incorporation into the membrane (see below); note that with 500 μM NPPB, current conduction is inhibited by >85% (Tombola et al., 1999b). These results are consistent with the assumption (although they do not prove it) that in the presence of this compound VacA channels are either in a blocked, nonconducting state or in a free, normally operating state.

For the sake of comparison, we examined the effects of another inhibitor and presumed blocker, DIDS, on the single-channel records. As shown in Fig. 4, DIDS apparently behaves much like NPPB, supporting the idea that both compounds produce a fast block. At a concentration of 100 μM in the *cis*/TAS (toxin addition side) compartment, rare full-size events could still be detected, suggesting a slower rate of inhibitor binding than with 50 μM NPPB.

We next examined the dependence of VacA inhibition on the side of addition of the inhibitor and on voltage. VacA inserts with a nonrandom orientation (Tombola et al., 1999a), and the oligomeric channel may be expected to be asymmetric with respect to the plane of the membrane, i.e., to present different energy barriers for blocker entry/exit at the two ends. Furthermore, a transmembrane potential (-40 mV) was applied in these experiments, which ought to influence the motion of the anionic inhibitors within the channel. We thus expected to observe steric and electrical effects leading to different extents of inhibition depending on whether the compounds were added to the *cis*/TAS or to the *trans* side. This was the case for DIDS and 4-acetanido-4′-isothiocyanatostilbene-2,2′-disulfonic acid (SITS) (Fig. 5 *A*), which inhibited to a greater extent when added on the TAS, indicating that access to the lumen from the opposite (*trans*) side was more difficult. Indeed, SITS had no effect at all when added in *trans*, providing definitive evidence for asymmetry and a 100% specific orientation of VacA channels in planar bilayers. However, to our surprise, NPPB inhibited to the same extent from either side, and the effects were additive, in the sense that the same percentage of inhibition was caused by a given concentration on one side or by a 50% lower concentration on both sides (Fig. 5 *D*). To analyze the voltage dependence of inhibition we used the rectification ratio, $|I^+/I^-|$, defined as the absolute value of the amplitude of the current flowing at a given *cis*/TAS-positive potential divided by that measured at the opposite voltage (under symmetrical salt conditions). This parameter offers the advantage that it can be measured accurately and repeatedly during an experiment even in the presence of continuing toxin incorporation, because sequential measurements at opposite voltages can be obtained with a time separation of milliseconds. The behavior observed by

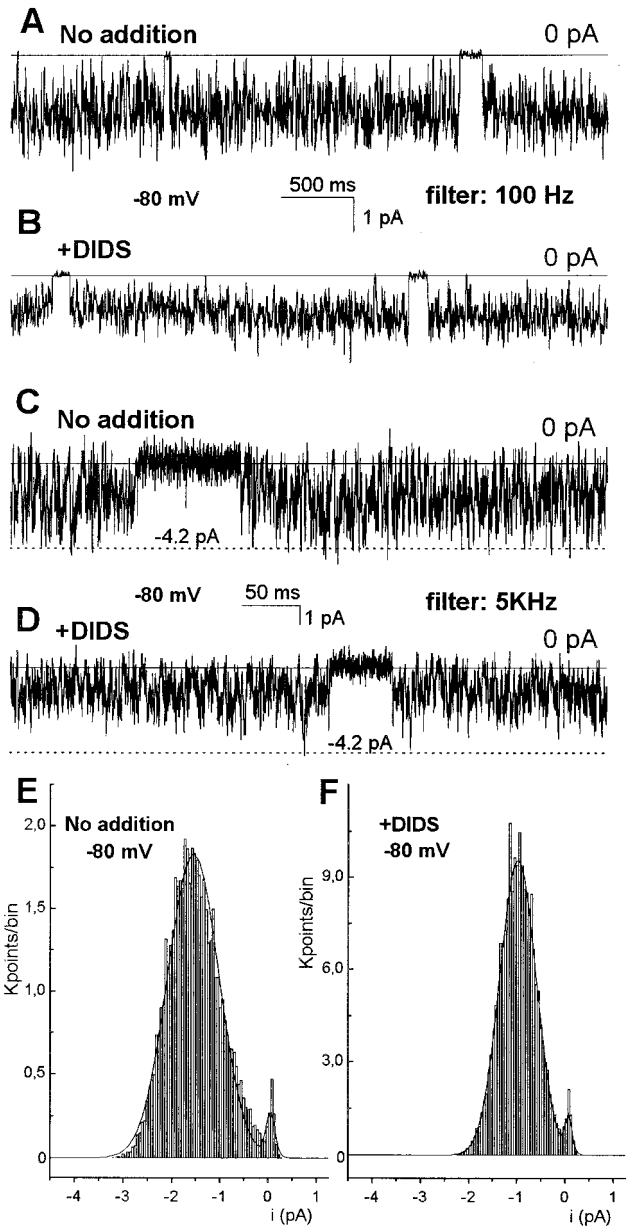

FIGURE 4 Inhibition of VacA single channels by DIDS. Experimental conditions as in Fig. 2. Illustrative current traces recorded in the absence (*A*) or presence (*B*) of 100 μM DIDS in the *trans* compartment. Filter: 100 Hz. Digital sampling: 1 KHz. V: -80 mV. (*C*) and (*D*) Traces from the same experiments as in (*A*) and (*B*), filtered at a corner frequency of 5 KHz and sampled at 50 KHz. (*E*) and (*F*) Amplitude histograms obtained from longer sections of the records illustrated in (A) and (*B*), respectively.

plotting $|I^+/I^-|$ versus the absolute value of the potential, $|V|$, is summarized by Fig. 5, *B*, *C*, *E*, and *F*. In the absence of inhibitors, the ratio is always <1 and it decreases with $|V|$ (Tombola et al., 1999a), as indicated by the dashed line, reflecting the intrinsic voltage dependence of the channel. With 200 μM DIDS in the *cis*/TAS compartment (Fig. 5 *B*, triangles) the ratio becomes >1 and the slope of the plot

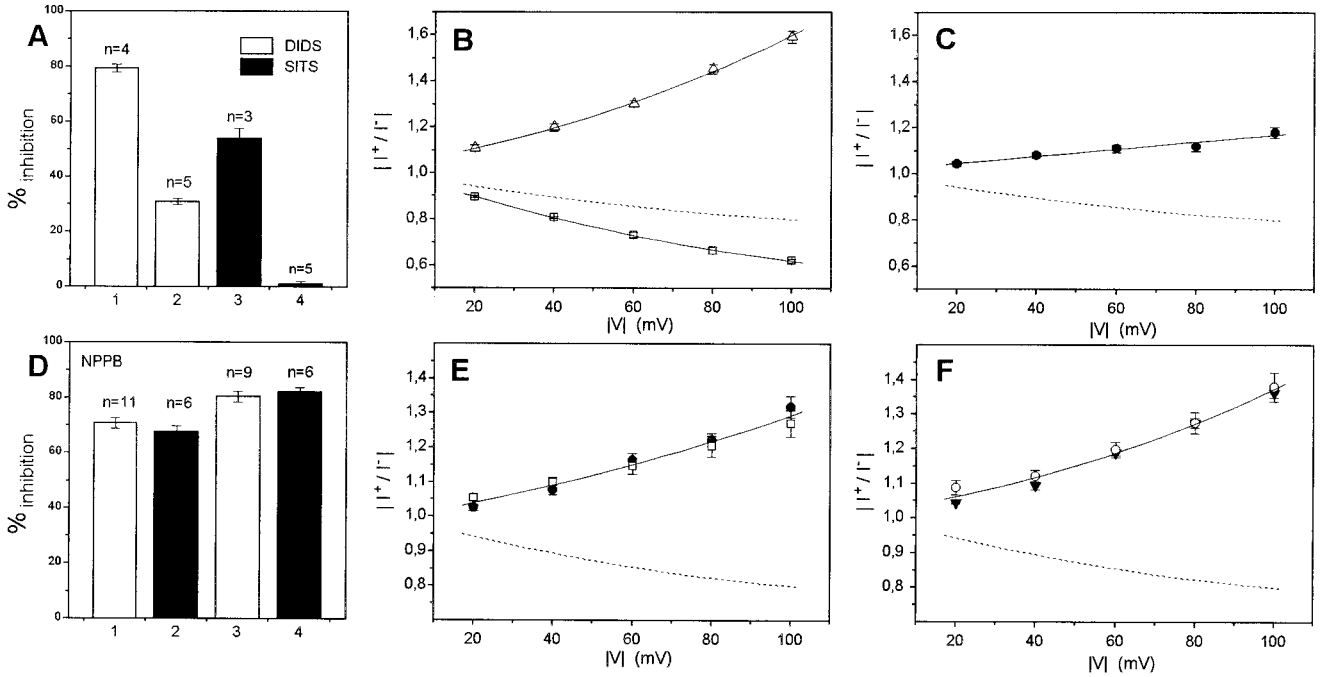

FIGURE 5 Side-of-addition- and voltage-dependence of inhibition by SITS, DIDS, and NPPB. (*A*) Percent inhibition of current conduction by VacA by 200 μM DIDS added to the *cis* (column 1) or *trans* (2) side and by 200 μM SITS in *cis* (3) or *trans* (4) $V = -40$ mV. The number of determinations (from separate experiments) averaged is indicated. (*B*) Plot of the rectification index $|I^+/I^-|$ vs. $|V|$ measured with 200 μM DIDS in *cis* (*triangles*) or *trans* (*squares*). The *dotted line* shows the best fit of the analogous plot in the absence of inhibitors (Tombola et al., 1999a). (*C*) As in (*B*), with 200 μM DIDS in both *cis* and *trans* compartments. (*D*) Percent inhibition of current conduction by 100 μM NPPB in *cis* (column 1) or *trans* (2), by 200 μM NPPB in *cis* (3) and by 100 μM NPPB in both the *cis* and *trans* compartments (4) $V = -40$ mV. (*E*) As in (*B*), with 100 μM NPPB in *cis*/TAS (*dark circles*) or *trans* (*open squares*). (*F*) As in (*B*), with 200 μM NPPB in *cis* (*dark triangles*) or 100 μM NPPB in both *cis* and *trans* chambers (*open circles*). All experiments were conducted in symmetrical 500 mM KCl. VacA was added to the *cis* compartment. Error bars indicate SE. For (*B*), (*C*), (*E*), and (*F*), the data plotted represent the average of 4 to 7 independent determinations.

versus $|V|$ becomes positive. A less marked and opposite change is observed when the inhibitor is added in *trans*. These results can be interpreted in terms of a block involving the migration of the negatively charged blocker along the channel lumen. When the inhibitor is present in the *cis* compartment, *cis*-positive voltages hinder its migration to the binding site within the VacA pore, while *cis*-negative voltages favor it. Exit to the *cis* side, presumably the major route in view of the restriction on the *trans* side, is expected to be favored by *cis*-positive potentials, and slowed by opposite voltages. As a result, current conduction is inhibited more at negative than at positive voltages. The converse holds when DIDS is present in *trans* (Fig. 5 *B*, *squares*). With DIDS in both compartments at the same concentration an intermediate curve with a positive slope was obtained, reflecting the prevalence of inhibition from the *cis* side (Fig. 5 *C*). To evaluate the relative intrinsic ease of access by DIDS to its blocking site from the two sides, we measured the inhibition of current conduction at 0 mV in the presence of a KCl gradient ([KCl] = 0.5 M in the DIDS-containing chamber, 2 M in the opposite one). Under these conditions 200 μM DIDS inhibited by 86.6 $\pm$ 2.4% ($n = 3$) when present on the same side as the toxin, and by 31.7 $\pm$ 3.1% ($n = 5$) when added on the opposite one.

The behavior observed with NPPB was also, in this case, strikingly different: irrespective of whether the compound was added in *cis*/TAS or *trans*, with 100 μM inhibitor the rectification ratio was >1, the slope of the plot $|I^+/I^-|$ vs. $|V|$ was positive, and the data obtained under the two conditions were coincident within experimental error (Fig. 5 *E*). Thus, the rectification ratio was voltage-dependent, but it was not influenced by the choice of the side of addition of NPPB. Furthermore, the same extent of inhibition at the various voltages, i.e., the same $|I^+/I^-|$ vs. $|V|$ plot, was obtained with a given concentration of NPPB in one compartment, or with a 50% lower concentration in both compartments, as exemplified in Fig. 5 *F*.

The curves relating $|I^+/I^-|$ to $|V|$ depended on [inhibitor] (added to the *cis*/TA side) as shown in Fig. 6 *A* for NPPB and Fig. 6 *B* for DIDS.

To explain the voltage dependence of inhibition by NPPB one can formulate two hypotheses: 1) NPPB binding is itself voltage-independent but causes the channel to adopt a subconductance state having the appropriate voltage depen-

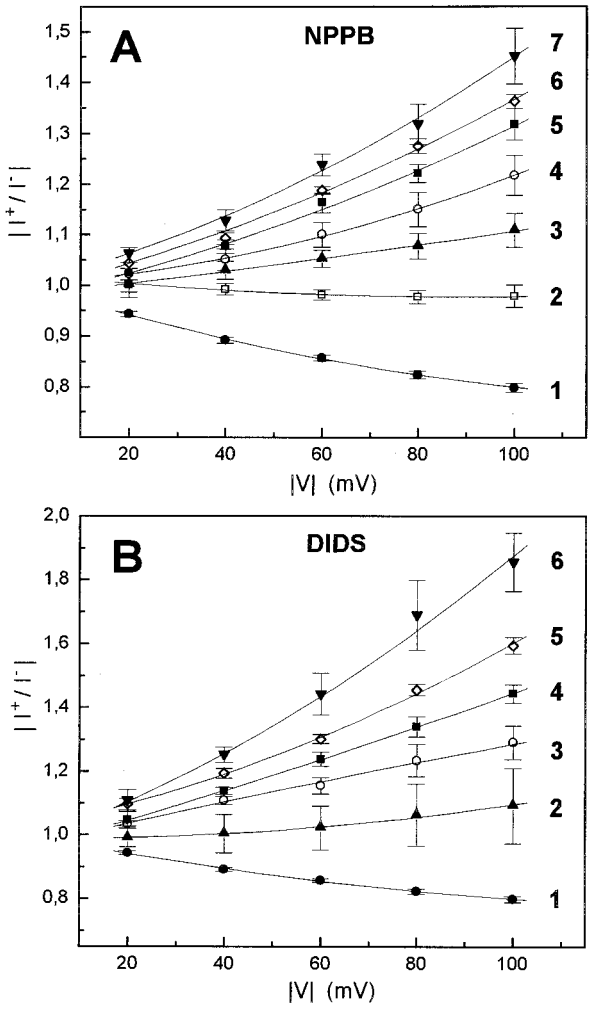

FIGURE 6 $|I^+/I^-|$ vs. $|V|$ plots at various concentrations of NPPB (*A*) and DIDS (*B*). (*A*) Plots analogous to those presented in Fig. 5, *B*, *C*, *E*, and *F*, obtained with $[NPPB]_{cis}$ = 0, 10, 20, 50, 100, 200, and 500 μM for curves 1–7, respectively. Conditions as for Fig. 5. (*B*) Plots as in (*A*) for DIDS. $[DIDS]_{cis}$ = 0, 20, 50, 100, 200, and 500 μM for curves 1–6, respectively. Data are the averages ±SE of 3 to 5 (NPPB) or 3 to 8 (DIDS) independent determinations, except for curve 1 in both (*A*) and (*B*), for which n = 15–16.

dence (opposite to that of the full conductance state). This subconductance state would carry about 12% as much current as the fully conductive state, as discussed above. 2) NPPB binding, i.e., the K_d of the binding equilibrium, is voltage-dependent.

The voltage dependence of the putative substate would be given by the $|I^+/I^-|$ vs. $|V|$ plot at maximum inhibition (curve 7 in Fig. 6 *A*). From the curve and the conductance attributed to the substate, one can thus calculate what rectification ratio should characterize any given partially inhibited population. The calculated and observed $|I^+/I^-|$ values are discrepant in all cases (except, of course, that of maximal inhibition), thus making hypothesis 2) above more likely.

K_d is linked to the fraction of ligated (i.e., blocked, in our scheme) channels, θ, by Langmuir's isotherm (e.g., Hille, 1992):

$$\theta = 1/(1 + K_d/[L]), \quad \text{or} \quad (1 - \theta) = K_d/(K_d + [L]) \tag{3}$$

where [L] is the concentration of ligand. In the presence of blocker:

$$\begin{aligned} |I^+/I^-| &= |(i^+/i^-)| * (P_o^+/P_o^-) * [(1 - \theta)^+/(1 - \theta)^-] \\ &= |I^+/I^-|_0 * [(1 - \theta)^+/(1 - \theta)^-] \end{aligned} \tag{4}$$

where the + or − superscripts refer to the application of a *cis*-positive or *cis*-negative voltage of a given magnitude, i is the current conducted by a single unblocked channel, P_o is the open probability, defined here as the probability of finding the unblocked channel in the open state, i.e., as the P_o of the channel in the absence of inhibitors. $(1 - \theta)$ is the fraction of blocker-free channels, and $|I^+/I^-|_0$ is the rectification ratio in the absence of inhibitor. Substituting (3) into (4):

$$\begin{aligned} |I^+/I^-| &= |I^+/I^-|_0 * \{[K_d^+/(K_d^+ + [L])]/[K_d^-/(K_d^- + [L])]\} \\ &= |I^+/I^-|_0 * \{([L]/K_d^- + 1)/([L]/K_d^+ + 1)\} \\ &= |I^+/I^-|_0 * \Phi \end{aligned} \tag{5}$$

with:

$$\Phi = |I^+/I^-|/|I^+/I^-|_0 = \{([L]/K_d^- + 1)/([L]/K_d^+ + 1)\} \tag{6}$$

where L stands for NPPB or DIDS. Fig. 7, *A* and *B*, shows plots of Φ vs. [L] for five values of $|V|$. The data have been interpolated using Eq. 6 to obtain estimates of K_d at the various voltages, and the values thus obtained are plotted as a function of the voltage applied in the *cis* chamber in Fig. 7, *C* and *D*. The plots are biphasic: in both cases K_d values increase with increasing potential in the positive range.

It was also of interest to investigate whether NPPB and DIDS would exclude each other from their inhibiting site. In the two extreme cases a) the binding of one inhibitor at its blocking site completely prevents binding of the other inhibitor at its site, which might or might not be the same (mutually exclusive binding), or b) each inhibitor can bind to its blocking site regardless of the presence of the other, and with unaltered equilibrium constants (independent binding). The percentage of inhibition (or percentage of residual current) resulting from application of a cocktail of two inhibitors can be predicted for each of the two models from chemical principles and from the experimentally determined inhibition caused by each inhibitor alone. The result of the relevant experiments, performed with 50 μM NPPB + 100 μM DIDS (*cis*/TAS) and summarized in Table 1, is in good agreement with the prediction based on the mutually exclusive binding model, indicating that the binding of DIDS at its blocking site prevents block by NPPB, and vice versa.

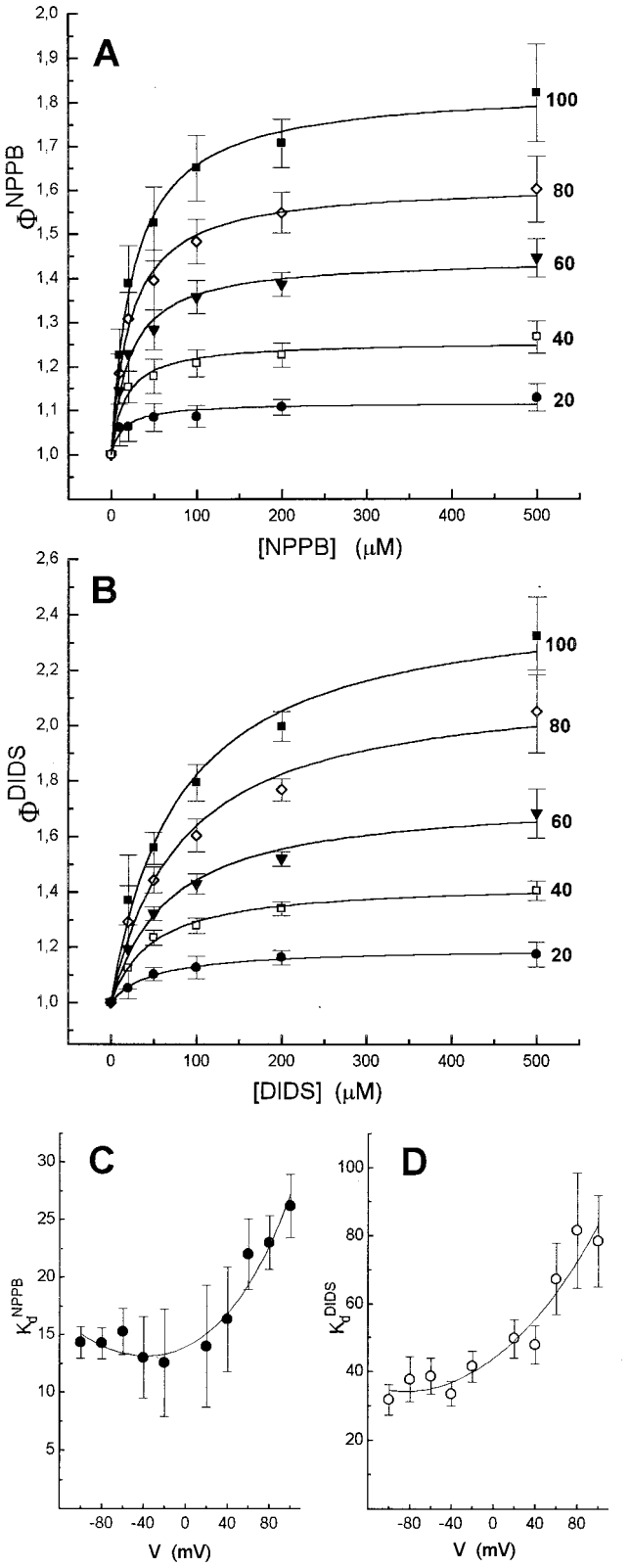

FIGURE 7 Voltage dependence of the dissociation constants of NPPB and DIDS. (*A*) Plots of Φ (defined in text) vs. [NPPB] for the |V| values specified at the right of each curve (± SE, n = 3–5). Interpolation according to Eq. 6 yields K_d estimates at the various voltages. (*B*) Plots of Φ vs. [DIDS] (± SE, n = 3–8) analogous to that reported in (*A*). (*C*) K_d^{NPPB} estimates from the fits in (*A*) plotted vs. V and fitted according to Eq. 7. The fit shown has $\delta = 0.6$ and $b_{off}^{cis}/b_{off}^{trans} = 1.4$ (see text). (*D*) K_d^{DIDS} estimates from the fits in (*B*) plotted vs. V and fitted according to Eq. 8. Error bars in (*C*) and (*D*) are standard deviations from the fits in (*A*) and (*B*).

TABLE 1 Competition experiments

Inhibitors	Residual current %	n
50 μM NPPB (*cis*)	37.0 ± 2.0	9
100 μM DIDS (*cis*)	32.4 ± 2.6	4
100 μM DIDS + 50 μM NPPB predicted for mutually exclusive sites	20.8 ± 1.7	
100 μM DIDS + 50 μM NPPB predicted for independent sites	12.0 ± 1.6	
100 μM DIDS + 50 μM NPPB experimental value	23.3 ± 2.3	5

This supports the notion that the binding sites for the two blockers are located on the inside surface of the pore.

DISCUSSION

To rationalize the observations, we introduce the hypothesis that NPPB reaches the blocking site within the VacA channel mainly by a voltage-independent and side-of-addition-independent pathway, presumably by entering the lumen of the oligomeric channel from the lipid bilayer, after partitioning into the latter from either the *cis* or the *trans* aqueous phase. The rate of access and binding to the blocking site from the aqueous phases, $k_{on}^{cis}*[NPPB]_{cis} + k_{on}^{trans}*[NPPB]_{trans}$, is considered to be negligible in comparison to $k_{on}^{memb}*[NPPB]_{memb}$. NPPB is an amphipathic molecule that would be fully expected to dissolve into a phospholipid bilayer, and similar compounds permeate biological membranes (McCarty et al., 1993; Schultz et al., 1999). The partition factor between an aqueous solution and the polar aprotic solvent chloroform is 1:12 (92.3% of NPPB is extracted from a 100 μM solution in 500 mM KCl, 10 mM HEPES, pH 7.2, by an equal volume of chloroform). Decane, an apolar liquid, is not a good solvent compared to water (5.9% of NPPB is extracted), suggesting that in the membrane NPPB might associate to a considerable extent with the polar headgroups of phospholipids rather than residing in the apolar inner region. If NPPB partitioning into the membrane is a diffusional process, its concentration in the bilayer would depend, simply through a proportionality factor at least in the lower concentration range, on the mean concentration in the aqueous compartments bathing the membrane, i.e., exposing the membrane to a given concentration C on one side and to NPPB-free medium on the other would be equivalent to exposing it to [NPPB] = C/2 on both sides, thus explaining the data in Fig. 5, *D* and *F*. To account for the effects of voltage, NPPB is postulated to

leave the binding site at least in part via voltage-dependent pathways, namely along the channel. Because the voltage dependence is relatively weak, however, it is possible that voltage-independent return to the membrane constitutes an important "off" pathway.

In the proposed scheme, the rate of NPPB binding to the blocking site, given essentially by $k_{on}^{memb}*[NPPB]_{memb}$, is not voltage sensitive, as is also the reverse process, whereas the constants for unbinding and exiting through the channel, k_{off}^{cis} and k_{off}^{trans}, are. Voltage thus affects the apparent dissociation constant of the blocker, which, given the assumptions made, can be defined as $K_d(V) = (k_{off}^{memb} + k_{off}^{cis}(V) + k_{off}^{trans}(V))/k_{on}^{memb} = (n_{free}/n_{bound})*[NPPB]_{memb}$, where n_{free} and n_{bound} are the numbers of free and NPPB-blocked channels in the membrane, respectively. Based on the results obtained with SITS and DIDS, the VacA channel appears to be more readily accessible from the TA than from the *trans* side. We may therefore expect NPPB exit to the TAS to be favored, i.e., at least in the absence of a transmembrane electrical field, $k_{off}^{cis} > k_{off}^{trans}$. The application of increasingly positive potentials in *cis* should accelerate the rate of exit, thus decreasing the overall apparent affinity of NPPB for its binding site and increasing k_{off}^{cis} and the K_d, as observed. *Cis*-negative potentials would be expected to hinder the migration of $NPPB^-$ toward the *cis* side, thus decreasing k_{off}^{cis}. k_{off}^{trans} is conversely expected to increase. The data in Fig. 7 *C* indicate at most a modest increase of K_d as V_{cis} is made more negative. Factors that might contribute to this behavior are steric hindrance to exit of NPPB to the *trans* (non-TA) side (i.e., a low pre-exponential term for k_{off}^{trans}, b_{off}^{trans}, in Eq. 7 below), and a weak voltage dependence of k_{off}^{trans}, if the binding site is in a deep position in the transmembrane field with respect to the *cis*/TAS aqueous phase. Using Woodhull's two symmetrical barriers model (Woodhull, 1973; Hille, 1992) the data in Fig. 7 *C* can be fitted with the equation:

$$\begin{aligned} K_d &= (k_{off}^{memb} + k_{off}^{cis} + k_{off}^{trans})/k_{on}^{memb} \\ &= [k_{off}^{memb} + b_{off}^{cis} * \exp(-\delta zFV/2RT) \\ &\quad + b_{off}^{trans} * \exp((1-\delta)zFV/2RT)]/k_{on}^{memb} \end{aligned} \tag{7}$$

where δ is the "electrical distance" of the binding site from the *cis* aqueous phase, b_{off}^{cis} (b_{off}^{trans}) is the rate constant for exit to the *cis* (*trans*) side at 0 applied voltage and the other symbols have the usual meanings. The fit of the data in Fig. 7 *C* with Eq. 7 is optimized with $\delta = 0.6$ and $b_{off}^{cis}/b_{off}^{trans} = 1.4$. However, only slightly worse fits are obtained with higher δ values and lower $b_{off}^{cis}/b_{off}^{trans}$ ratios, in the range $0.6 \le \delta \le 0.9$ ($1.4 \ge b_{off}^{cis}/b_{off}^{trans} \ge 0.3$). The observed voltage dependence may thus be accounted for by any of a number of possible combinations envisioning a binding site located more/less deeply (with respect to the TAS) in the channel, together with a more/less intrinsically easy exit toward the *trans* side (compared to exit to the TA side). In any case, the NPPB binding site can safely be localized as closer to the *trans*- than to the TAS pore end, since no reasonable fitting curve can be obtained when imposing $\delta \le 0.5$.

For channel block by DIDS (present only on the *cis*/TA side), K_d is given by:

$$\begin{aligned} K_d &= (k_{off}^{cis} + k_{off}^{trans})/k_{on}^{cis} \\ &= [b_{off}^{cis} * \exp(-\delta zFV/2RT) \\ &\quad + b_{off}^{trans} * \exp((1-\delta)zFV/2RT)] \\ &\quad \div b_{on}^{cis} * \exp(\delta zFV/2RT) \end{aligned} \tag{8}$$

The fit of the data in Fig. 7 *D* is best with $\delta \approx 0.19$ and $b_{off}^{cis}/b_{off}^{trans} \approx 8.4$, and rapidly worsens as these values are changed. Imposing $\delta \ge 0.5$ leads to utter fitting failure. Thus, DIDS appears to bind close to the *cis*-side "mouth," and the binding sites for DIDS and NPPB are likely to be distinct.

Because of the principle of microscopic reversibility, if NPPB can exit the pore via its water-filled interior, the channel lumen ought also to provide an access path to the blocking site(s). The model envisioned, however, considers this diffusional process to be much less efficient than inhibitor supply via the hydrophobic pathway. Some evidence supporting the existence of an aqueous pathway is provided by the titration curves relating current conduction to $[NPPB]_{cis}$ (Tombola et al., 1999b). As mentioned, the data show the presence of an uninhibitable current accounting for approximately 12% of total (Tombola et al., 1999b). Incomplete block hypothesis (see above) aside, this component might be tentatively explained by proposing that the membrane becomes saturated with NPPB at some [NPPB] $< 500\ \mu M$, and that under these saturation conditions the rate of NPPB entry into the channel via the hydrophobic pathway is about 7.3 times as high as the overall exit rate. The fit of the titration data (Tombola et al., 1999b, Fig. 2) improves somewhat (not shown) if a second component is added, i.e., if the equation used becomes:

$$\%_{r.c.} = 100 - P_1/(1 + K_{d1}/[L]) - P_2/(1 + K_{d2}/[L]) \tag{9}$$

Optimization yields $P_1 = 82.3 \pm 3.6$, $P_2 = 100$, $K_{d1} = 16.0 \pm 1.8\ \mu M$, $K_{d2} = 5.8 \pm 3.4$ mM, consistent with the presence of a parallel low-affinity inhibition process leading to complete channel block at high $[NPPB]_{cis}$. The characteristics of this presumptive low-affinity inhibition could not be investigated further, because of the limited solubility of the compound. Clearly, at any rate, it would not contribute appreciably to the form of the voltage dependence curves and rectification index vs. $|V|$ relationships.

The data allow us to propose a working model of VacA block, schematized in Fig. 8. It should be made clear that this model applies to VacA, and it is not meant to be generally valid. The major points may be summarized as follows:

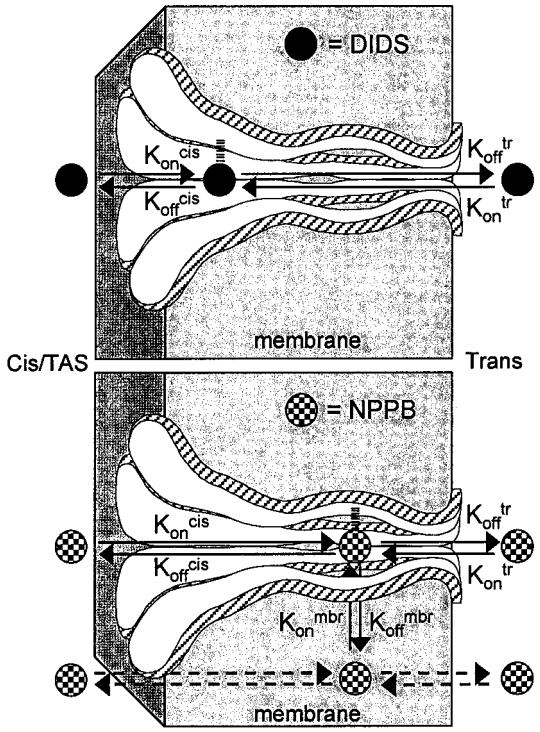

FIGURE 8 A working model of the VacA channel and of the processes involved in block. An imaginary depiction of a cross-section of a VacA hexamer, illustrating the pathways for block by DIDS (*upper panel*) and NPPB. Inside the channel, the blockers are positioned at the approximate location of the blocking sites. The rate constants for the various binding equilibria are indicated. The length of the corresponding *arrows* is arbitrary and is not meant to reflect the relative magnitudes of the constants.

NPPB blocks the VacA channel mainly by reaching a binding site exposed onto the channel lumen after partitioning into the lipid bilayer, in a voltage-independent process that presumably involves permeation at the interface between the channel-forming monomers. In turn this implies a loose packing of the monomers and a flexible channel structure, consistent with the high rates of the (undefined) conformational transitions responsible for pore flickering. The blocking site is situated in the *trans* (non-TAS) half of the channel. Unblocking involves at least in part voltage-affected migration along the aqueous pore. More hydrophilic compounds such as SITS and DIDS behave as more classical blockers, entering the channel through its open extremities. Of these, the one at the TAS end offers an easier pathway for both entry and exit. Although NPPB and DIDS cannot be simultaneously present in the pore, their binding sites do not overlap, the one for DIDS being located in the *cis*/TAS half of the channel. The equilibria involved in blocking are fast, implying a high rate of channel clearance. To account for the voltage independence of blocking, one may propose that NPPB diffuses from the bilayer into the channel as the undissociated acid, which would release its proton upon reaching the aqueous channel lumen, acquiring a negative charge which would favor its prompt expulsion in the presence of an electrical field. The planar membrane with inhibitor on one side only is an out-of-equilibrium system in which a flow of NPPB from one compartment to the other takes place. If diffusion of $NPPB^-$ from the bulk aqueous phase to the membrane/solution interface were the kinetically limiting process (i.e., much slower than protonation and subsequent diffusion of NPPBH into the membrane and then to the other side or into the channel), as seems quite possible, the concentration of NPPBH in the membrane would be expected to be proportional to the average [$NPPB^-$] in the aqueous phases (*cis* and *trans* compartments), in agreement with the behavior illustrated in Fig. 1 (curve *b*).

The possibility that arylaminobenzoates might reach their binding site through the membrane phase has been mentioned (McCarty et al., 1993; Schultz et al., 1999) but it has not, to our knowledge, been investigated in detail. An analogous scheme has instead been supported for the inhibition of cation-selective channels by local anesthetics (e.g., Hille, 1992). The ability of amphipathic blockers such as NPPB to follow a hydrophobic path to (and probably from) the blocking site may well explain some of the characteristics of the block of other anion channels by these compounds. It is relevant in this context that ClC-family pores are also believed to have an oligomeric structure (e.g., Lorenz et al., 1996), which may facilitate entry of the inhibitor into the channel lumen.

This work is in partial fulfillment of the requirements for a Doctorate degree in Cellular and Molecular Biology and Pathology by Francesco Tombola. We thank Dr. Ildikò Szabò and Prof. Cesare Montecucco for many useful discussions and for critically reading the manuscript, and Dr. Federica Oregna for performing part of the experiments. The financial support by CNR, Progetto Finalizzato Biotecnologie (97.01168.PF 49), and by Telethon grant A.59 is gratefully acknowledged.

REFERENCES

Alberts, B., D. Bray, J. Lewis, M. Raff, K. Roberts, and J. D. Watson. 1994. Molecular Biology of the Cell, 3rd ed. Garland Publishing. New York and London.

Altan, N., Y. Chen, M. Schindler, and S. M. Simon. 1999. Tamoxifen inhibits acidification in cells independent of the estrogen receptor. *Proc. Natl. Acad. Sci. USA.* 96:4432–4437.

Bezrukov, S. M., I. Vodyanoy, and V. A. Parsegian. 1994. Counting polymers moving through a single ion channel. *Nature.* 370:279–281.

Buyse, G., T. Voets, J. Tytgat, C. De Greef, G. Droogmans, B. Nilius, and J. Eggermont. 1997. Expression of human pI_{Cln} and ClC-6 in *Xenopus* oocytes induces an identical endogenous chloride conductance. *J. Biol. Chem.* 272:3615–3621.

Cover, T. L., and M. J. Blaser. 1992. Purification and characterization of the vacuolating toxin from *Helicobacter pylori. J. Biol. Chem.* 267: 10570–10575.

Cover, T. L., P. I. Hanson, and E. J. Heuser. 1997. Acid-induced dissociation of VacA, the *Helicobacter pylori* vacuolating cytotoxin, reveals its pattern of assembly. *J. Cell Biol.* 138:759–769.

Czajkowsky, D. M., H. Iwamoto, T. L. Cover, and Z. Shao. 1999. The vacuolating toxin from *Helicobacter pylori* forms hexameric pores in lipid bilayers at low pH. *Proc. Natl. Acad. Sci. USA.* 96:2001–2006.

de Bernard, M., E. Papini, V. de Filippis, E. Gottardi, J. L. Telford, R. Manetti, A. Fontana, R. Rappuoli, and C. Montecucco. 1995. Low pH activates the vacuolating toxin of *Helicobacter pylori*, which becomes acid and pepsin resistant. *J. Biol. Chem.* 270:23937–23940.

Dick, G. M., K. K. Bradley, B. Horowitz, J. R. Hume, and K. M. Sanders. 1998. Functional and molecular identification of a novel chloride conductance in canine colonic smooth muscle. *Am. J. Physiol.* 275: C940–C950.

Furukawa, T., O. Takehiko, K. Yoshifumi, and M. Hiraoka. 1998. Characteristics of rabbit ClC-2 current expressed in *Xenopus* oocytes and its contribution to volume regulation. *Am. J. Physiol.* 274:C500–C512.

Garner, J. A., and T. L. Cover. 1996. Binding and internalization of the *Helicobacter pylori* vacuolating cytotoxin by epithelial cells. *Infect. Immun.* 46:4197–4204.

Hille, B. 1992. Ionic Channels of Excitable Membranes, 2nd ed. Sinauer Assoc., Sunderland, MA.

Iwamoto, H., D. M. Czajkowsky, T. L. Cover, G. Szabo, and Z. Shao. 1999. VacA from *Helicobacter pylori*: a hexameric chloride channel. *FEBS Lett.* 450:101–104.

Lanzavecchia, S., P. L. Bellon, P. Lupetti, R. Dallai, R. Rappuoli, and J. L. Telford. 1998. Three-dimensional reconstruction of metal replicas of the *Helicobacter pylori* vacuolating cytotoxin. *J. Struct. Biol.* 121:9–18.

Leunk, R. D., P. T. Johnson, B. C. David, W. G. Kraft, and D. R. Morgan. 1988. Cytotoxic activity in broth-colture filtrates of *Campylobacter pylori. J. Med. Microbiol.* 26:93–99.

Linsdell, P., and J. W. Hanrahan. 1996. Flickery block of single CFTR chloride channels by intracellular anions and osmolytes. *Am. J. Physiol.* 271:C628–C634.

Lorenz, C., M. Pusch, and T. J. Jentsch. 1996. Heteromultimeric CLC chloride channels with novel properties. *Proc. Natl. Acad. Sci. USA.* 93:13362–13366.

Lupetti, P., J. E. Heuser, R. Manetti, P. Massari, S. Lanzavecchia, P. L. Bellon, R. Dallai, R. Rappuoli, and J. L. Telford. 1996. Oligomeric and subunit structures of the *Helicobacter pylori* vacuolating cytotoxin. *J. Cell Biol.* 133:801–807.

Manetti, R., P. Massari, D. Burroni, M. de Bernard, A. Marchini, R. Olivieri, E. Papini, C. Montecucco, R. Rappuoli, and J. L. Telford. 1995. *Helicobacter pylori* cytotoxin: importance of native conformation for induction of neutralizing antibodies. *Infect. Immun.* 63:4476–4480.

McCarty, N. A., S. McDonough, B. N. Cohen, J. R. Riordan, N. Davidson, and H. A. Lester. 1993. Voltage-dependent block of the cystic fibrosis transmembrane conductance regulator Cl^- channel by two closely related arylaminobenzoates *J. Gen. Physiol.* 102:1–23.

Molinari, M., C. Galli, N. Norais, J. L. Telford, R. Rappuoli, J. P. Luzio, and C. Montecucco. 1997. Vacuoles induced by *Helicobacter pylori* toxin contain both late endosomal and lysosomal markers. *J. Biol. Chem.* 272:25339–25344.

Molinari, M., C. Galli, M. de Bernard, N. Norais, J. M. Ruysschaert, R. Rappuoli, and C. Montecucco. 1998. The acid activation of *Helicobacter pylori* toxin VacA: structural and membrane binding studies. *Biochem. Biophys. Res. Comm.* 248:334–340.

Montecucco, C., E. Papini, M. de Bernard, and M. Zoratti. 1999. Molecular and cellular activities of *Helicobacter pylori* pathogenic factors. *FEBS Lett.* 452:16–21.

Nilius, B., J. Sehrer, and G. Droogmans. 1994. Permeation properties and modulation of volume-activated Cl^- currents in human endothelial cells. *Br. J. Pharmacol.* 112:1049–1056.

Nilius, B., J. Prenen, G. Szücs, L. Wei, F. Tanzi, T. Voets, and G. Droogmans. 1997. Calcium-activated chloride channels in bovine pulmonary artery endothelial cells. *J. Physiol.* 498:381–396.

Papini, E., M. de Bernard, E. Milia, M. Zerial, R. Rappuoli, and C. Montecucco. 1994. Cellular vacuoles induced by *Helicobacter pylori* originate from late endosomal compartments. *Proc. Natl. Acad. Sci. USA.* 91:9720–9724.

Papini, E., B. Satin, C. Bucci, M. de Bernard, J. L. Telford, R. Manetti, R. Rappuoli, M. Zerial, and C. Montecucco. 1997. The small GTP binding protein rab7 is essential for cellular vacuolation induced by *Helicobacter pylori* cytotoxin. *EMBO J.* 16:15–24.

Papini, E., B. Satin, N. Norais, M. de Bernard, J. L. Telford, R. Rappuoli, and C. Montecucco. 1998. Selective increase of the permeability of polarized epithelial cell monolayers by *Helicobacter pylori* vacuolating toxin. *J. Clin. Invest.* 102:813–820.

Pelicic, V., J.-M. Reyrat, L. Sartori, C. Pagliaccia, R. Rappuoli, J. L. Telford, C. Montecucco, and E. Papini. 1999. *Helicobacter pylori* VacA cytotoxin associated to the bacteria increases epithelial permeability independently of its vacuolating activity. *Microbiology.* 145:2043–2050.

Satin, B., N. Norais, J. L. Telford, R. Rappuoli, M. Murgia, C. Montecucco, and E. Papini. 1997. Effect of *Helicobacter pylori* vacuolating toxin on maturation and extracellular release of procathepsin D and Epidermal Growth Factor degradation. *J. Biol. Chem.* 272: 25022–25028.

Schmid, A., R. Blum, and E. Krause. 1998. Characterization of cell volume-sensitive chloride currents in freshly prepared and cultured pancreatic acinar cells from early postnatal rats. *J. Physiol.* 513: 453–465.

Schmieder, S., S. Lidenthal, U. Banderali, and J. Ehrenfeld. 1998. Characterization of the putative chloride channel xClC-5 expressed in *Xenopus laevis* oocytes and comparison with endogenous chloride currents. *J. Physiol.* 511:379–393.

Schultz, B. D., A. K. Singh, D. C. Devor, and R. J. Bridges. 1999. Pharmacology of CFTR chloride channel activity. *Physiol. Rev.* 79: S109–S144.

Singh, A. K., G. B. Afink, C. J. Venglarik, R. P. Wang, and R. J. Bridges. 1991. Colonic Cl channel blockade by three classes of compounds. *Am. J. Physiol.* 261:C51–C63.

Szabò, I., Brutsche, S., Tombola, F., M. Moschioni, B. Satin, J. L. Telford, R. Rappuoli, C. Montecucco, E. Papini, and M. Zoratti. 1999. Formation of anion-selective channels in the cell plasma membrane by the toxin VacA of *Helicobacter pylori* is required for its biological activity. *EMBO J.* 18:5517–5527.

Telford, J. L., P. Ghiara, M. Dell'Orco, M. Comanducci, D. Burroni, M. Bugnoli, M. F. Tecce, S. Censini, A. Covacci, Z. Xiang, E. Papini, C. Montecucco, L. Parente, and R. Rappuoli. 1994. Gene structure of the *Helicobacter pylori* cytotoxin and evidence of its key role in gastric disease. *J. Exp. Med.* 179:1653–58.

Tilmann, M., K. Kunzelmann, U. Frobe, I. Cabantchik, H. J. Lang, H. C. Englert, and R. Greger. 1991. Different types of blockers of the intermediate-conductance outwardly-rectifying chloride channel in epithelia. *Pflügers Arch.* 418:556–563.

Tombola, F., C. Carlesso, I. Szabò, M. de Bernard, J.-M. Reyrat, J. L. Telford, R. Rappuoli, C. Montecucco, E. Papini, and M. Zoratti. 1999a. *Helicobacter pylori* vacuolating toxin forms anion-selective channels in planar lipid bilayers: possible implication for the mechanism of cellular vacuolation. *Biophys. J.* 76:1401–1409.

Tombola, F., F. Oregna, S. Brutsche, I. Szabò, G. Del Giudice, R. Rappuoli, C. Montecucco, E. Papini, and M. Zoratti. 1999b. Inhibition of the vacuolating and anion channel activities of the VacA toxin of *Helicobacter pylori*. *FEBS Lett.* 460:221–225.

Verveen, A. A., and L. J. De Felice. 1974. Membrane noise. *Progr. Biophys. Mol. Biol.* 28:189–265.

von Weikersthal, S. F., M. A. Barrand, and S. B. Hladky. 1999. Functional and molecular characterization of a volume-sensitive chloride current in rat brain endothelial cells. *J. Physiol.* 516:75–84.

Woodhull, A. M. 1973. Ionic blockage of sodium channels in nerve. *J. Gen. Physiol.* 61:687–708.

Yahiro, K., T. Niidome, M. Kimura, T. Hatakeyama, H. Aoyagi, H. Kurazono, K. Imagawa, A. Wada, J. Moss, and T. Hirayama. 1999. Activation of *Helicobacter pylori* VacA toxin by alkaline or acidic conditions increases its binding to a 250-kDa receptor protein-tyrosine phosphatase. *J. Biol. Chem.* 274:36693–36699.